Crystal Growth of Transition Metal Fluorides

Norikazu OHTORI,† Yuzo YOSHIKAWA,* Ken-ichi SASAKI,†† Hisaki MORIWAKI, and Haruhiko YOKOYAMA†††
Department of Chemistry, Faculty of Science, Okayama University, Tsushima, Okayama 700
†Department of Electronic Chemistry, Tokyo Institute of Technology, Nagatsuta, Midori-ku, Yokohama 227
††Faculty of General Education, Rikkyo University, Toshima-ku, Tokyo 171
†††Department of Chemistry, Yokohama City University, Kanazawa-ku, Yokohama 236
(Received September 14, 1989)

Kinetics of crystal growth of transition-metal fluorides, MF_2 ($M=Zn^{II}$ and Pb^{II}) has been studied by the use of both constant composition and conventional methods. The effective orders in an empirical reaction-rate function of supersaturation were 1.71 (2.0) for $ZnF_2 \cdot 4H_2O$ and 0.88 (1.2) for PbF_2 (The values in the parentheses are from the conventional method). These findings suggest that the crystals of zinc fluoride grow by a spiral growth (surface reaction) mechanism and lead fluoride by a bulk diffusion controlled mechanism.

Since the well known BCF theory was reported,[1] many experimental techniques have been developed to measure crystal-growth rates with a high precision and the growth mechanisms have been discussed. Among the recent investigations in aqueous solution systems, the gravimetric technique for various inorganic salts and computer simulations by Bennema et al.,[2] the potentiometric technique for sparingly soluble alkaline earth salts by Nancollas et al.,[3,5–7] and the in situ observation method for $Ba(NO_3)_2$ by Sunagawa et al.,[4] can be cited as representatives.

The crystal growth mechanism of a series of fluoride salts of the alkaline earths have been kinetically studied in the seeded aqueous-solution systems by Nancollas et al.[5–7] We extend the studies to divalent transition-metal fluoride crystals and investigate the correlation between the types of crystal growth and the structure of the crystals.

The rates of the crystallization were measured by using the constant composition and the conventional methods. The constant composition method which requires a continual monitoring of the supersaturated solutions can be readily applied to the present salts by the use of a reliable fluoride-ion selective electrode. Solutions containing the lattice ions are automatically added into a precipitating phase maintaining supersaturation constant, while, in the conventional method, the supersaturation decreases during the crystallization and must be determined by taking samples at appropriate intervals.

Experimental

All chemicals were of reagent grade. Potassium nitrate, zinc nitrate hexahydrate, and lead nitrate were recrystallized twice from water. Potassium fluoride was purified by two-time recrystallization of potassium hydrogen fluoride from water, followed by removing hydrogen fluoride on heating on a platinum plate under nitrogen. Stock solutions of KF and $M(NO_3)_2$ (M=Zn and Pb) were prepared using doubly distilled water. Potassium ion concentration was determined by exchanging for hydrogen ion on Dowex-50 ion-exchanger column and titrating the liberated acid. The KF solution was stored in polyethylene bottles. Transition metal ion concentrations in the stock solutions and samples taken at conventional runs were determined by chelatometric titration with EDTA. The slope of the tangent to the resulting crystal-growth curve is the growth rate at each time with the corresponding supersaturation.

Seed crystals were prepared with an apparatus as shown in Fig. 1. The solutions of potassium fluoride and transition-metal nitrate were added by dropping to doubly distilled water with top-stirring in order to prevent the crystals from being ground and under a nitrogen atmosphere in order to eliminate the carbonate formation. The precipitated seed crystals were washed with saturated solutions of the corresponding metal fluorides and were allowed to age in a Teflon bottle for at least one month at 25 °C before use. In crystallization experiments, the seed crystals were added as a slurry.

The specific surface areas (SSA) of the seed crystals measured by using a BET method through nitrogen adsorption, were 1.4 and 1.3 $m^2 \cdot g^{-1}$ for $ZnF_2 \cdot 4H_2O$ and PbF_2, respectively.

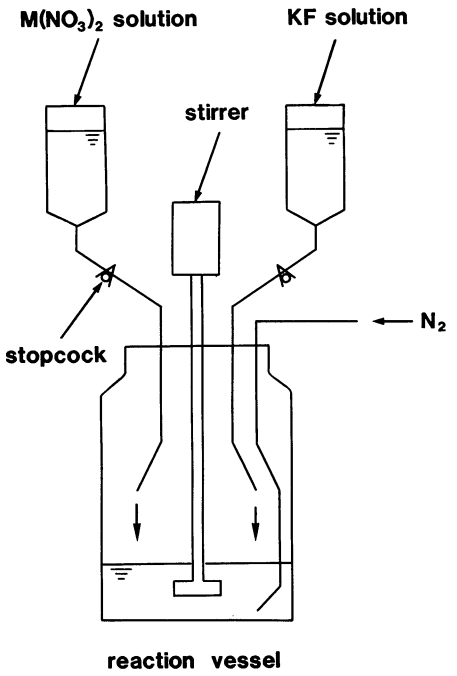

Fig. 1. Apparatus to prepare the seed crystals.

Crystal growth was studied with the constant composition and conventional methods under a nitrogen atmosphere using a round-bottomed polyethylene cell of 500 ml capacity. The round bottomed shape was selected in order to avoid the seed crystals stagnating at the bottom corner of the ordinary beaker. The cell was maintained at 25 °C by circulating thermostated water through the outer jacket. Stirring was effected using a variable-speed stirrer with top-loading propeller.

Supersaturated solutions of metal fluorides were prepared at 25 °C by mixing solutions of metal nitrate and potassium fluoride in the range as wide as possible of relative supersaturation, σ defined as follows:

$$\sigma = (a_{MF_2}{}^{1/3} - a^{\circ}_{MF_2}{}^{1/3})/a^{\circ}_{MF_2}{}^{1/3}, \quad (1)$$

Table 1. Experimental Conditions of Crystal-Growth Kinetics of PbF_2

Run	Total lead	Seeds	Supersaturation
	10^{-3} mol·dm^{-3}	g	σ
1	4.463	0.123	0.379
2	4.448	0.144	0.375
3	4.228	0.143	0.316
4	4.230	0.137	0.318
5	3.973	0.133	0.249
6	3.984	0.129	0.252
7	3.731	0.162	0.183
8	3.731	0.157	0.183
9	3.487	0.155	0.116
10	3.487	0.151	0.116
11	3.240	0.135	0.0466
12	3.240	0.159	0.0466

Table 2. Experimental Conditions of Crystal-Growth Kinetics of $ZnF_2 \cdot 4H_2O$

Run	Total zinc	Seeds	Supersaturation
	10^{-1} mol·dm^{-3}	g	σ
1	1.093	0.141	0.547
2	1.093	0.141	0.547
3	0.9939	0.141	0.432
4	0.9939	0.141	0.432
5	0.8946	0.141	0.314
6	0.8946	0.141	0.314
7	0.7952	0.424	0.190
8	0.7952	0.424	0.190
9	0.6958	0.424	0.0654
10	0.6958	0.565	0.0654

where a_{MF_2} and $a^{\circ}_{MF_2}$ are the activities of the metal fluorides in the supersaturated and saturated solutions, respectively.

The supersaturation ratio, σ in Eq. 1 was determined on the basis of the concentrations of ionic species in each supersaturated solution which was calculated in terms of successive approximations and by considering equations of mass balance, electroneutrality, and the formation of the various species associated with the equilibria (Table 3).

In the constant composition method, by the automatic injection of two titrant solutions consisting of metal nitrate and potassium fluoride from mechanically coupled burets, the concentrations of metal fluoride and the back-ground electrolyte were kept constant by following addition of seed crystals to supersaturated solutions. Seed crystals were added as a slurry after thermal equilibration for the supersaturated solution. The rate of titrant addition was controlled by monitoring emf of a specific fluoride-ion selective electrode (Orion Model 94-09) through a Hiranuma Reporting Titrator (COMTITE-8) which was modified to control mechanically coupled burets. The crystal-growth rate was calculated from the rate of addition of the titrant solutions.

The fluoride electrode was coupled with an electrolytic silver/silver chloride reference electrode with double junctions of liquid.[6]

The present potentiostat system controlled changes in supersaturation ratio within 1% during crystallization reactions.

All the experimental conditions are listed in Tables 1 and 2. The ratio of fluoride to metal ions was kept to be 2 for every run.

The solid phase collected during the experiment was inspected using a scanning electron microscope (SEM: Akashi ALPHA-30). The samples were taken from the seeded growth mixtures as a slurry or from the stocked seed slurries. The slurries were filtered with a Millipore filter paper (0.22 μm) under suction and air-dried. Before being placed in the microscope, the dried samples (1 cm×1 cm) were coated using a vacuum deposition method with 200-Å (for PbF_2) and 400-Å (for $ZnF_2 \cdot 4H_2O$) layers of Au for electric conduction.

Other experimental details are similar to those in the previous paper.[6]

Similar experiment for crystal growth of MnF_2 (SSA=0.4 $m^2 \cdot g^{-1}$) was carried out, but reproducible results were not obtained because of high stickiness of MnF_2 crystals.

Results and Discussion

Figures 2 and 3 show typical growth curves, the slopes of which are related to the rate of crystallization,

Table 3. Thermodynamic Data for Complex Formation and Solubility Product (25 °C)

Reaction	Thermodynamic equilibrium constants	Ref.
$H^+ + F^- \rightleftharpoons HF$	1510	12
$HF + F^- \rightleftharpoons HF_2^-$	3.39	12
$Zn^{2+} + F^- \rightleftharpoons ZnF^+$	13.8	13
$Zn^{2+} + 2F^- \rightleftharpoons ZnF_2(s)$	8.19×10^{-5}	This work
$Zn^{2+} + OH^- \rightleftharpoons ZnOH^+$	4.36×10^{4}	14
$Pb^{2+} + F^- \rightleftharpoons PbF^+$	64.4	15
$Pb^{2+} + 2F^+ \rightleftharpoons PbF_2(s)$	3.13×10^{-8}	This work
$Pb^{2+} + OH^- \rightleftharpoons PbOH^+$	5.48×10^{6}	16

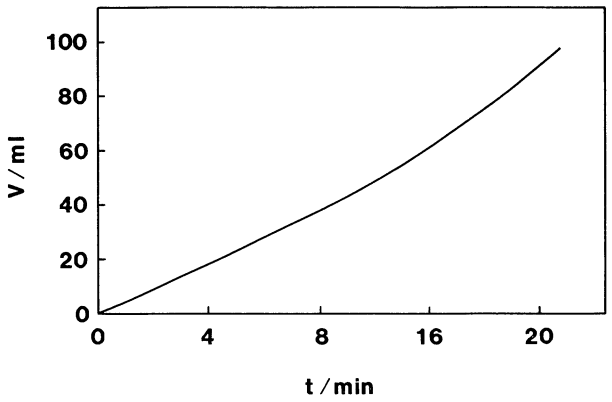

Fig. 2. A typical crystal-growth curve of lead fluoride: σ=0.379 (see Table 1).

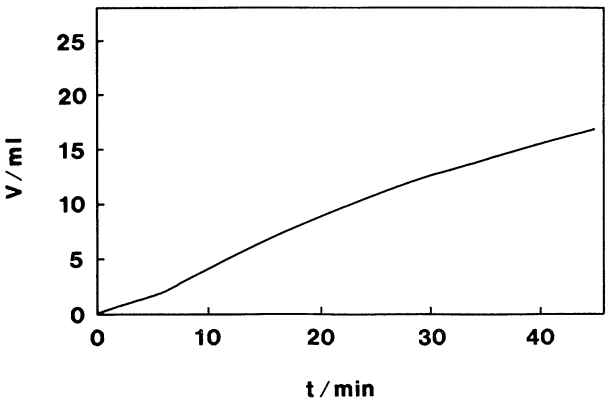

Fig. 3. A typical crystal-growth curve of zinc fluoride: σ=0.314 (see Table 1).

for the constant composition methods in the $ZnF_2 \cdot 4H_2O$ and PbF_2 systems, respectively.

It is expected that the rate is proportional to the active surface area of seed crystals as will be mentioned later. The rate for lead fluoride gradually increased with time, while that for zinc fluoride decreased after halfway. Therefore, the rate data for zinc fluoride were obtained from the curves up to about 40% of growth. The decrease may be attributed to aggregation of the seed crystals in the course of the crystallization owing to the stickiness of them. The increase of the rate for lead fluoride was slower than that estimated assuming an isotropic growth process, which is understood based on the SEM observation as will be described later.

By analogy of the results of previous crystallization studies,[5-7] the rate of crystal growth can be expressed by

$$R' = k \cdot s \cdot \sigma^n. \quad (2)$$

In this equation, k is the rate constant for crystal growth, s is a function of the surface area related to the number of active sites of growth on the added seed

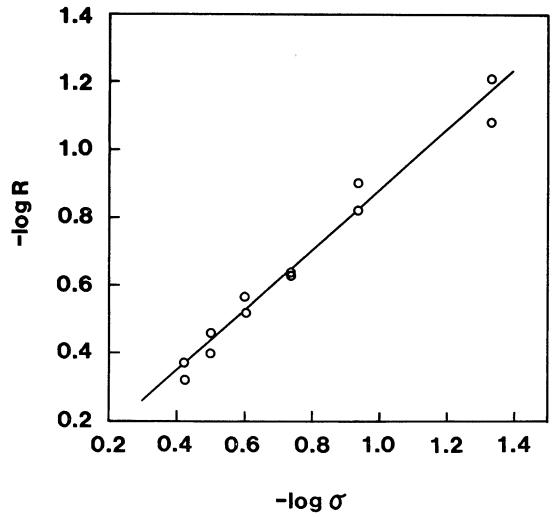

Fig. 4. Plots of $-\log(\text{Rate})$ against $-\log \sigma$ for crystal growth of lead fluoride.

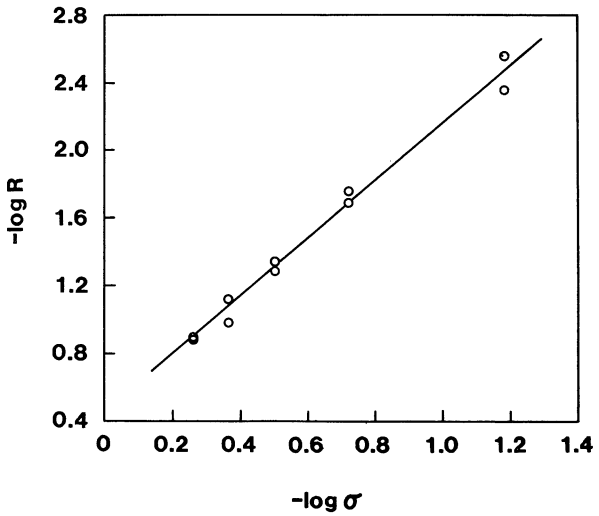

Fig. 5. Plots of $-\log(\text{Rate})$ against $-\log \sigma$ for crystal growth of zinc fluoride.

crystals, and n is the effective order of reaction. Further, a normalized growth rate per unit area is expressed by

$$R = R'/s = k \cdot \sigma^n. \quad (3)$$

The value of n can be obtained from plots of $-\log R$ as a function of $-\log \sigma$.

Figures 4 and 5 show $-\log R$ vs. $-\log \sigma$ plots for each system. The n's obtained from the slopes are 0.88 ± 0.04 and 1.71 ± 0.07, for PbF_2 and $ZnF_2 \cdot 4H_2O$, respectively. In these cases, the corrections were not made for changes of surface areas, because only initial and nearly linear parts of growth curves were used for analysis.

From the conventional method, 1.2 ± 0.1 and 2.0 ± 0.1 were obtained for n's of PbF_2 and $ZnF_2 \cdot 4H_2O$,

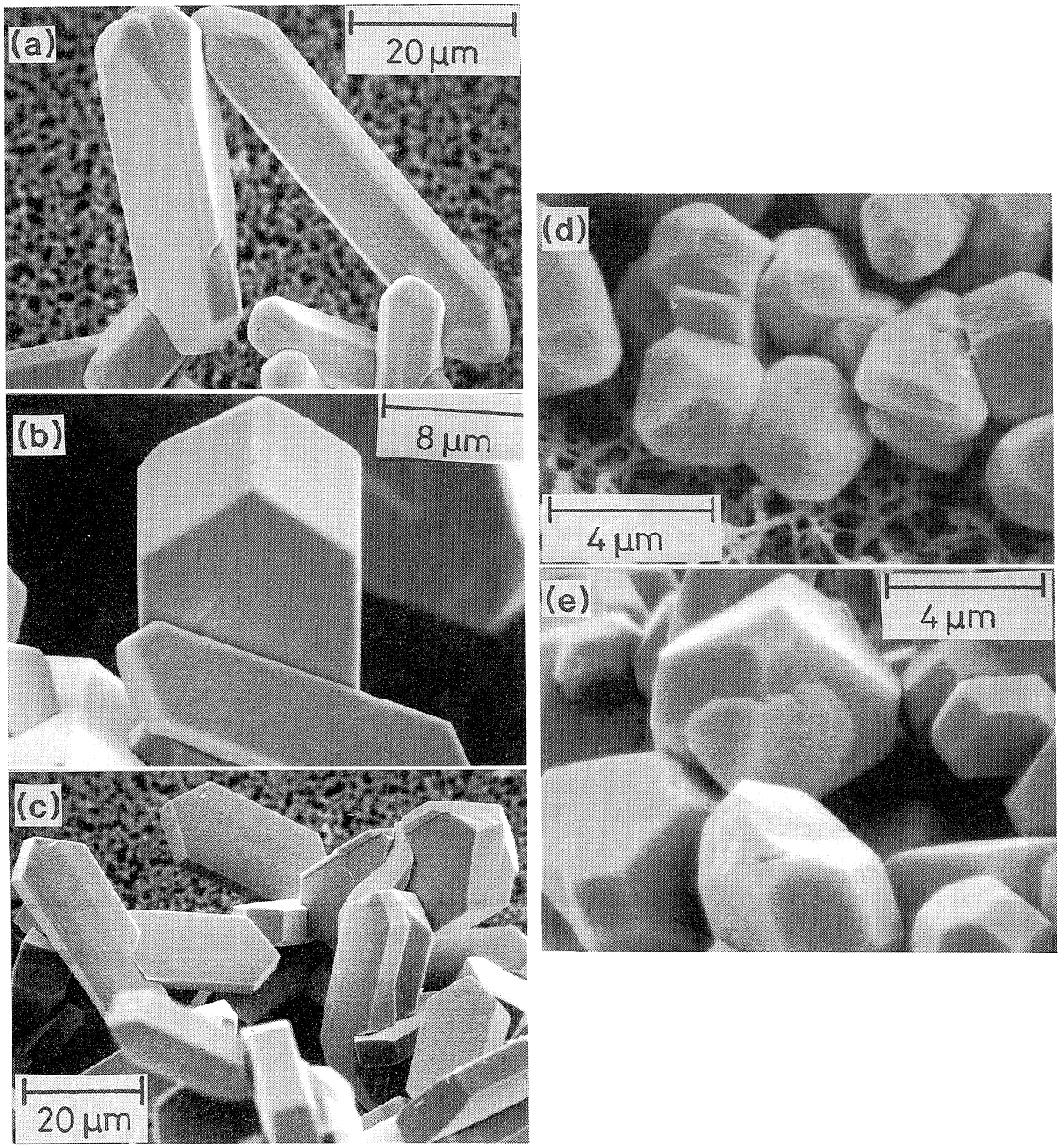

Fig. 6. Scanning-electron-micrographic views of the seed crystals. (a) initial seeds, (b) 20%-grown seeds, (c) 80%-grown seeds for lead fluoride, (d) initial seeds, (e) 70%-grown seeds for zinc fluoride.

respectively. The measured values by the two different methods agreed approximately.

Figure 6 shows scanning electron micrographs of the solids taken from both the seeded crystallization systems of lead and zinc fluorides at various times. From the micrographs of PbF_2, a growth process may be depicted as shown in Fig. 7. That is to say, the seed crystals are columnar and their corners are rounded, the 20%-grown crystals have angular corners, and the 80%-grown crystals are plate-like. Thus, it is seen that growth rates to particular directions are much faster than the others, which means that the active surface area on the seed crystals is less than that estimated for the isotropically-grown crystals. On the other hand, the crystals of $ZnF_2 \cdot 4H_2O$ change only sizes keeping similar proportion of the form.

If a crystallization process is entirely diffusion-controlled, the growth rate can be represented by

$$R_1 = k_1 \cdot \sigma. \tag{4}$$

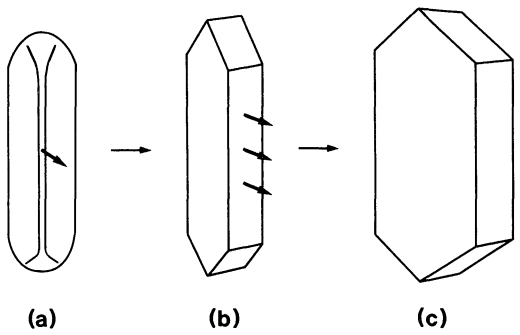

Fig. 7. Schematic views for the growth of PbF_2 seed crystals. (a) initial, (b) 20%-grown, (c) 80%-grown seeds.

In the case of surface-reaction-controlled growth, Frank derived Eq. 5 by considering spiral growth where kink (active) sites can be continuously provided, and by solving a diffusion equation:[8]

$$R_2 = k_2 \cdot \sigma \cdot \gamma \tag{5}$$

In these equations, k_1 and k_2 are constants, and γ is called crystal growth affinity of a driving force for crystal growth and is expressed as follows:

$$\gamma = \Delta\mu/RT = \ln(\sigma + 1), \tag{6}$$

where $\Delta\mu$ is the excess chemical potential of solute in a supersaturated solution over that in saturated solution.

On the other hand, Gilmer and Bennema obtained Eq. 7 from their polynuclear growth (birth and spread) model and the cation dehydration mechanism.[9]

$$R_3 = k_3 \cdot \gamma^{1/6} \cdot \sigma^{2/3} \cdot e^{-B/\gamma} \tag{7}$$

In this quation, $B/\gamma = \Delta G^*/kT$, where ΔG^* is the excess free energy of the two-dimensional critical nucleus formation on the crystal surface. B can be estimated with

$$B = (1/3)\pi\bar{h}^{-2}\{\ln(c_x/c_s)\}^2, \tag{8}$$

where $\bar{h}$ is the average number of water molecules surrounding a precipitating cation and anion in a solution, and c_x and c_s are the concentrations of the solute in pure crystals and of that in a saturated solution, respectively.[10]

In order to compare the growth rate equations derived from these hypothetical growth mechanisms with those from the present experimental results, Eqs. 5 and 7 were arranged as follows:

The results of the growth reaction rates with $k_2 = k_3 = 10^{-3}$ are presented as plots of $-\log R$ vs. $-\log \sigma$ in Fig. 8. The spiral growth models by Frank yields almost linear plots (full line) over an extensive σ range

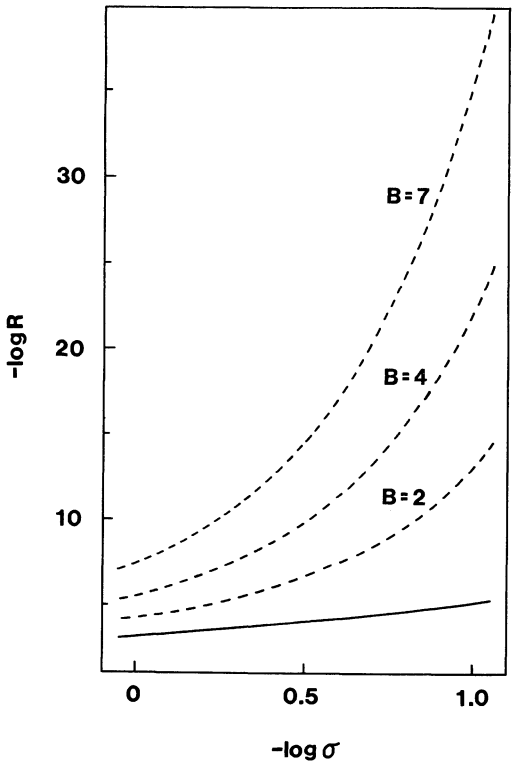

Fig. 8. Plots of $-\log R$ against $-\log \sigma$. Full line for R_2 (Eq. 5); broken line for R_3 (Eq. 7).

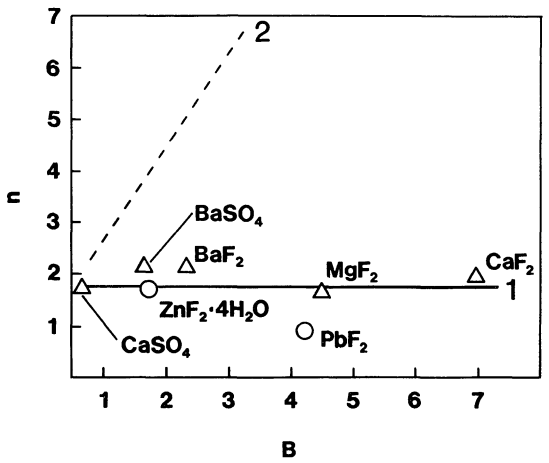

Fig. 9. The slope, n, as a function of B in the region of σ=0.2—0.5. Full line 1 for R_2 (Eq. 5); broken line 2 for R_3 (Eq. 7).

with $n \approx 1.8$. In contrast, the plots in the polynuclear model are curved depending upon the value of σ for each B. Since n is the slope of curves, it varies with σ and B.

Since for many sparingly soluble salts, plots of $-\log R$ as a function of $-\log \sigma$ often show good linearity, the n's were determined as effectively constant values in the limited region of supersaturation (σ=0.2—0.5). Figure 9 shows the plots of n vs. B

within the limited region. A zone around line 1 corresponds to a spiral (or adsorption layer) growth mechanism and zone around line 2 to a birth and spread or polynuclear mechanism. As can be seen from Fig. 9, the obtained experimental point for the crystal growth of $ZnF_2 \cdot 4H_2O$ is close to line 1, suggesting a spiral growth mechanism. In contrast, since the point for PbF_2 is apart from two lines and obeys Eq. 4, it can be considered that the crystals grow by a bulk diffusion controlled mechanism.

It was found from Figs. 6 and 7 that the rate of growth to particular directions is much faster than the others in PbF_2 crystals. The growth rate may correlate with the crystal structure. PbF_2 has a $PbCl_2$-type crystal structure,[11] where a (100) face contains only Pb^{2+} ions or only halide anions, alternately, whereas (010) and (001) faces necessarily contain Pb^{2+} and halide ions in the ratio of 1 to 2. Therefore, species on the (100) face is unstable and much more active for crystal growth than the others. This can be correlated with the above-mentioned finding about growth rate difference in the crystal faces.

We would like to express grateful acknowledgments to Prof. Hideo Yamatera (Daido institute of Technology) for helpful discussions, to Mss. Masae Takeuchi and Mariko Kimura for their contributions to preliminary experiments, and to Dr. Yasuo Nakanishi for help in the use of a scanning electron microscope. The work was supported by Grants-in-Aid for Scientific Research (Nos. 58540383 and 63470039) from the Ministry of Education, Science and Culture, for which the authors' thanks are due.

One of the authors (Y. Y.) wishes to thank Professor G. H. Nancollas (State University of New York at Buffalo) for his giving the chance and guidance in crystal growth researches.

References

1) W. K. Burton, N. Cabrera, and F. C. Frank, *Phil. Trans. Roy. Soc. (London)*, **A243**, 299 (1951).

2) a) P. Bennema, Journal of The Japanese Association of Crystal Growth, **4**, 135 (1977); b) P. Bennema, *J. Cryst. Growth*, **69**, 182 (1984), and references cited therein.

3) a) G. H. Nancollas, *Adv. Colloid Interface Sci.*, **10**, 215 (1979); b) D. J. White and G. H. Nancollas, *J. Cryst. Growth*, **57**, 267 (1982); c) J. C. Heughebaert, S. J. Zawacki, and G. H. Nancollas, *ibid.*, **63**, 83 (1983), and references cited therein.

4) a) K. Tsukamoto, H. Ohba, and I. Sunagawa, *J. Cryst. Growth*, **63**, 18 (1983); b) K. Maiwa, K. Tsukamoto, and I. Sunagawa, *ibid.*, **82**, 611 (1987), and references cited therein.

5) G. H. Nancollas, R. A. Bochner, E. Liolios, L. J. Shyu, Y. Yoshikawa, J. P. Barone, and D. Svrjcek, *AIChE Symp. Ser.*, **78**, 26 (1982).

6) Y. Yoshikawa and G. H. Nancollas, *J. Cryst. Growth*, **64**, 222 (1983).

7) Y. Yoshikawa, G. H. Nancollas, and J. Barone, *J. Cryst. Growth*, **69**, 357 (1984).

8) G. M. van Rosmalen, P. J. Daudey, and W. G. J. Marchée, *J. Cryst. Growth*, **52**, 801 (1981).

9) G. H. Gilmer and P. Bennema, *J. Appl. Phys.*, **432**, 1347 (1972).

10) O. Söhnel, J. Garside, and S. J. Jančić, *J. Cryst. Growth*, **39**, 307 (1977).

11) A. F. Wells, "Structural Inorganic Chemistry," 4th ed. Clarendon Press, Oxford (1975), p. 222.

12) A. J. Ellis, *J. Chem. Soc.*, **1963**, 4300.

13) R. O. Cook, A. Davies, and L. A. K. Stavely, *J. Chem. Thermody.*, **3**, 907 (1971).

14) F. Achenza, *Ann. Chim.*, **48**, 565 (1958).

15) A. M. Bond, *Analyt. Chim. Acta*, **53**, 159 (1971).

16) Å. Olin, *Acta Chem. Scand.*, **14**, 126 (1960).